www.amlett.com, www.vbripress.com/aml, DOI: 10.5185/amlett.2016.6106 Published online by the VBRI Press in 2016

Photocatalytic characteristics for the nanocrystalline TiO_2 supported on $Sr_4Al_{14}O_{25}:Eu^{2+}$, Dy^{3+} phosphor beads

Hyun-Je Sung[1], Byung-Min Kim[1], Sang-Chul Jung[2] and Jung-Sik Kim[1]*

[1]*Department of Materials Science and Engineering, The University of Seoul, Seoul, 130-743 Korea*
[2]*Department of Environmental Engineering, Sunchon National University, Jeonnam, 540-742 Korea*

*Corresponding author. Tel: (+82) 2-6490-2409; E-mail: jskim@uos.ac.kr

Received: 21 August 2015, Revised: 19 November 2015 and Accepted: 05 December 2015

ABSTRACT

The photocatalytic behaviors of TiO_2-supported on the long lasting phosphor beads were examined. Nanocrystalline TiO_2 was coated on ellipsoidal-spherical beads of an alkaline earth aluminate phosphor, $Sr_4Al_{14}O_{25}:Eu^{2+}$, Dy^{3+}, by low pressure chemical vapor deposition (LPCVD). The photocatalytic reaction was examined by measuring the decomposition of benzene and toluene gases by gas chromatography under ultraviolet, visible light (λ> 410 nm) irradiation, as well as in the dark. The LPCVD TiO_2-coated $Sr_4Al_{14}O_{25}:Eu^{2+}$, Dy^{3+} showed an active photocatalytic reaction under visible irradiation. The mechanisms of the photocatalytic reactivity for the TiO_2-coated $Sr_4Al_{14}O_{25}:Eu^{2+}$, Dy^{3+} phosphor beads were discussed in terms of the crystal structure at the interface, energy band structure and phosphorescence. The coupling of TiO_2 with the $Sr_4Al_{14}O_{25}:Eu^{2+}$, Dy^{3+} phosphor resulted in energy band bending in the junction region between TiO_2 and $Sr_4Al_{14}O_{25}:Eu^{2+}$, Dy^{3+} phosphor, which makes the TiO_2 crystal at the interface photo-reactive under visible light irradiation. The LPCVD TiO_2-coated $Sr_4Al_{14}O_{25}:Eu^{2+}$, Dy^{3+} phosphor beads were also photo-reactive in the dark through the light photons emitted from the $Sr_4Al_{14}O_{25}:Eu^{2+}$, Dy^{3+} phosphor.

Keywords: Photocatalyst; TiO_2; phosphor beads; $Sr_4Al_{14}O_{25}:Eu^{2+}$, Dy^{3+}; LPCVD.

Introduction

Titanium dioxide (TiO_2) is well known as one of the most promising photocatalysts with potential applications in various fields such as environmental remediation, photogeneration of hydrogen from water, self-cleaning systems, and solar energy utilization since it is non-toxic, offers physical and chemical stability, and has wide availability at a low price. However, the practical applications of TiO_2 as photocatalysts are still limited by the wide energy band gap (3.03 eV for rutile and 3.18 eV for anatase) that can only absorb approximately 3~5 % of sunlight in the ultraviolet (UV) region, and fast recombination rate of charge carriers [**1**].

Hence, considerable research efforts have been made to develop new photocatalysts to extend the light absorption of TiO_2 toward the visible region and to separate charge carriers of electrons and holes. The doping of noble metals (Pt, Rd, Ag, Au, etc.) or transition metals (Fe, Ni, Cr, Cu, V, Mn, etc.) as dopants enhanced the photocatalytic reactivity of TiO_2, remarkably [**2-5**]. Also, anion doping (N, S, F, Cl, C, etc.) into TiO_2 could shift the optical absorption edge from the UV range to the visible light range [**6, 7**].

The coupling of TiO_2 with other metal oxides, such as SiO_2, SnO_2, WO_3, In_2O_3, (Sr, La)$TiO_{3+\delta}$ and $ZnMn_2O_4$, altered the photocatalytic efficiency and energy range of photoexcitation [**8, 9**]. In addition, the junction of TiO_2 with other semiconductors with a narrow band gap such as CdS, Cu_2O, and Cu_2S enhanced the photocatalytic reactivity under visible light irradiation [**10, 11**]. Recently, the coupling of TiO_2 with light-emitting materials such as phosphors was known as another way to improve the photocatalytic reactivity of TiO_2 based composites. In this case, the luminescent phosphors can supply light photons activating the TiO_2 photocatalyst. Several long afterglow phosphors/TiO_2 or TiO_2−N composites showed active visible-light photocatalytic reaction which was partly assisted through luminescence from phosphors [**12-14**].

The long-lasting characteristics of Eu^{2+}-doped alkaline earth aluminate phosphors have attracted considerable attention for their potential applications in fields, such as luminous paints, safety indicators in emergency cases, electronic instrument dial pads, lighting apparatus and switches, automobile dials and panels, writing and printing inks, and plasma display phosphors[**15-17**]. The luminescence is strongly dependent on the host lattice, and can occur from the UV to the red region of the electromagnetic spectrum. Up to now, alkali-earth aluminate phosphors with excellent properties, such as $CaAl_2O_4$:(Eu^{2+},Nd^{3+}) [blue], $Sr_4Al_{14}O_{25}$:(Eu^{2+}, Dy^{3+}) [blue-green], $SrAl_2O_4$:(Eu^{2+}, Dy^{3+}) [green] and

$BaAl_2O_4$:(Eu^{2+}, Dy^{3+}) [blue], have been developed for a range of applications[**18, 19**].

Many applications of nanocrystalline TiO_2 such as a photocatalytic filter for water and air purification require the supporting of TiO_2 on the substrates. Various substrates have been used as a nanocrystalline TiO_2 support for the photocatalytic degradation of water, air and organic pollutants. For example, glass materials as glass mesh, glass fabric, glass wool and glass beads, carbon fibers and nanotubes, polymeric membranes, metal mesh, ceramic membranes, and zeolites were investigated as a TiO_2 support [**20-22**].

In this study, the photocatalytic reaction properties of titanium dioxide (TiO_2)-supported on the long phosphorescent materials were investigated. Nanocrystalline TiO_2 films were deposited on the spherical beads of phosphor, $Sr_4Al_{14}O_{25}$:Eu^{2+},Dy^{3+} by LPCVD with titanium(IV) isopropoxide (TTIP, $Ti[OCH(CH_3)_2]_4$) as a precursor. Then, the photocatalytic behaviors of TiO_2-suported on the phosphor beads were examined in terms of the photocatalytic degradation of benzene and toluene gases as volatile organic compounds (VOCs).

Experimental

Nanocrystalline TiO_2 thin films were deposited on the phosphor beads ($Sr_4Al_{14}O_{25}$:Eu^{2+}, Dy^{3+}) using a low-pressure CVD (LPCVD) system. TTIP ($Ti(OC(CH_3)_2)_4$, 99.99 %, UP Chem., Korea) and oxygen gas were used as the precursor and reaction gas for deposition, respectively. Argon gas was used as a carrier gas for TTIP at a flow rate of 125 sccm. The LPCVD reactor was constructed as a showerhead type. The liquid precursor was kept at 60°C in a bubbler placed in a heating jacket to ensure an even temperature distribution. The substrate deposition temperature was 400 °C and the pressure was maintained at 1 torr. The flow rate was controlled using a mass flow controller.

The $Sr_4Al_{14}O_{25}$:Eu^{2+}, Dy^{3+} phosphor was prepared by a conventional sintering process using the following raw materials: $Sr(NO_3)_2$ (99 %, Aldrich, USA), $Al(NO_3)_3{\cdot}9H_2O$(98 %, Kyoto Chem., Japan), Eu_2O_3 (99.99 %, Aldrich, USA), and Dy_2O_3(99.99 %, Aldrich, USA) with a molar ratio of 3.67:14:0.02:0.04. A small amount of B_2O_3 (3wt %) was added to the mixed powders as a flux. Raw powders were weighed appropriately, mixed in ethanol, and ground by a ball mill for 24 h. Then, well-mixed powders were calcined by heating at 1400 °C for 6 hrs in the reducing atmosphere of N_2-5 % H_2 gas mixture. The sintering process is described in detail elsewhere [**23, 24**].

To produce the phosphor beads, the synthesized phosphor powders were mixed with a gelated 4wt % sodium alginate ($C_5H_7O_4{\cdot}(COOH)_n$) solution using a stirrer, and was then dripped repeatedly into a 10wt % $CaCl_2$ solution through a 9 mm diameter nozzle. Subsequently, the semi-solidified phosphor beads were separated, dried at 100°C in a dry oven and heat-treated in a reduction atmosphere of 5%H_2-95%N_2 at 1,250°C for 5 hrs. The fabricated phosphor beads were the mixture of ellipsoidal and spherical shapes. **Fig. 1.** shows the photographs of fabricated $Sr_4Al_{14}O_{25}$:Eu^{2+}, Dy^{3+} phosphor beads taken at the day (a) and night (b). The phosphor beads glow as a blue-green color in darkness.

The photocatalytic reaction behavior of the LPCVD TiO_2-coated phosphors was examined by measuring the decomposition of benzene (or toluene) gas using a gas chromatography (GC) system. The photocatalytic reaction chamber was filled with 10 ppm benzene (or toluene) gas and irradiated with UV light [75-W mercury lamp] or a 100 W white light lamp (Sylvania incandescent lamp). In the case of visible light irradiation, a UV-light cut-off lens (Edmund Optics) was inserted just below the white light lamp to filter the UV-light with wavelengths (λ) < 410 nm. After a predetermined irradiation time, the sampling gas was extracted from the reaction chamber using a 1 *ml* syringe for the GC analysis test. The morphology, crystal structure and surface composition of the TiO_2-supported on the $Sr_4Al_{14}O_{25}$:Eu^{2+}, Dy^{3+} phosphor beads were characterized via scanning electron microscopy (SEM), transmission electron microscopy (TEM), energy dispersive spectroscopy (EDS), x-ray diffractometry (XRD), and Auger electron spectroscopy (AES), respectively.

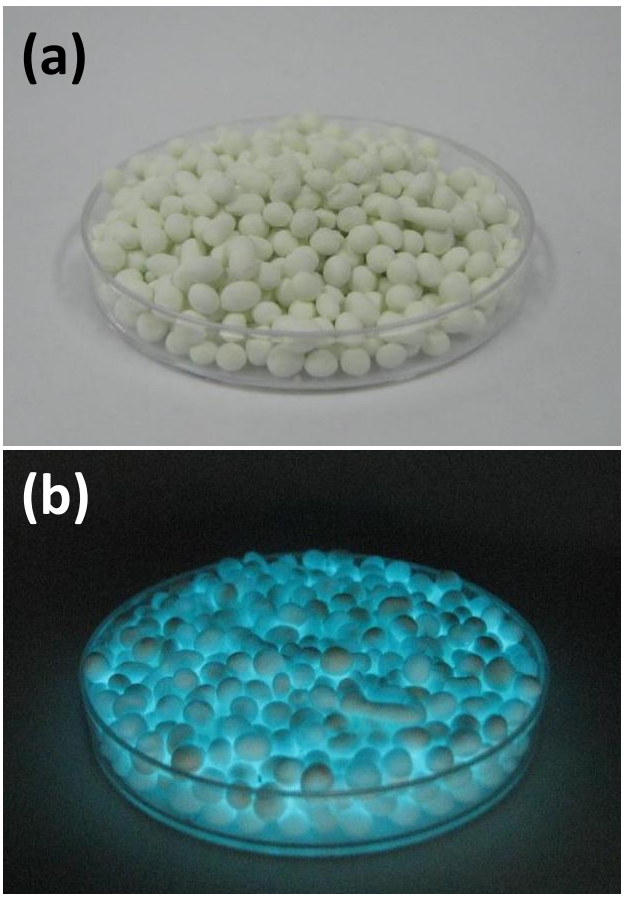

Fig. 1. Photographs of fabricated $Sr_4Al_{14}O_{25}$:Eu^{2+},Dy^{3+} phosphor beads taken at the day (a) and night (b).

Results and discussion

Fig. 2 shows the variation of XRD patterns of the LPCVD TiO_2-film deposited on the glass substrate over the deposition temperatures of 320, 350, and 400 ºC. The film thickness was typically about 100 nm. The matching of the observed and standard 'd' values (JCPDS 21-1272) confirmed that only anatase-phase diffraction peaks were

evident without any peaks of a rutile phase. In all the XRD spectra, the diffraction peaks correspond to the (101), (112), (200) and (211) crystal planes of the anatase phase, respectively. With increasing deposition temperature, the integrated intensity ratios of $I_{(112)}/I_{(101)}$ and $I_{(211)}/I_{(101)}$ increased, while the $I_{(002)}/I_{(101)}$ ratio decreased. It is probably that as the deposition temperature increases, the lateral growth of TiO_2 toward <200> direction decreases, while the columnar growth to <211> increases [**25**]. The (112)-preferred orientation has been reported to enhance the photocatalytic reactivity of anatase-TiO_2 [**26**].

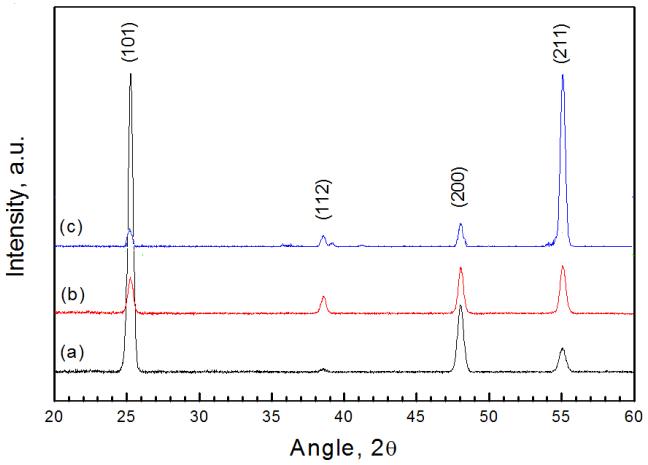

Fig. 2. XRD patterns of LPCVD-TiO_2 deposited at (a) 320°C, (b) 350°C, and (c) 400°C for 1min.

Fig. 3 shows (**a**) a cross-sectional TEM image (bright field) of TiO_2-coated $Sr_4Al_{14}O_{25}$:Eu^{2+}, Dy^{3+} phosphor, (b) the X-ray spectra obtained from energy dispersive spectroscopy (EDS) analysis at three different points marked at the TEM image in (a), and (c) lattice image observed around the interface. The peaks for Sr, Ti, Al and O elements were observed around the interface (point 2 in (a)) between TiO_2 and $Sr_4Al_{14}O_{25}$:Eu^{2+}, Dy^{3+} phosphor, indicating that the intermixing of Ti, Sr and Al occurred at the interface. As shown in the lattice image in (c), an interface layer of the Sr-Ti-O compounds (mostly $SrTiO_3$) was formed between the TiO_2 and $Sr_4Al_{14}O_{25}$:Eu^{2+}, Dy^{3+} phosphor. The crystallinity of the Sr-Ti-O intermetallic compound is partially amorphous because the lattice fringe image at the interface is not clear compared to the areas of $Sr_4Al_{14}O_{25}$:Eu^{2+}, Dy^{3+} phosphor and TiO_2, and its orientation random and irregular due to its typical amorphous structure. This is because TiO_2 was deposited at 400 °C, which is less than the temperature for the complete crystallization of Sr-Ti-O compounds, such as $SrTiO_3$, 725 °C [**27**]. Considering the TEM lattice image **Fig. 3(a)** and EDS spectra, the points marked as "1", "2" and "3" at **Fig. 2**(**a**) correspond to the areas of the TiO_2 film, Sr-Ti-O compounds (mostly $SrTiO_3$) and $Sr_4Al_{14}O_{25}$:Eu^{2+}, Dy^{3+} phosphor, respectively.

Fig. 4(a) shows the changes in the benzene concentration with an irradiation time for the TiO_2 coated phosphor ($Sr_4Al_{14}O_{25}$:Eu^{2+}, Dy^{3+}) beads under either UV or visible light irradiation. As shown in the figure for comparison, the benzene concentration for the TiO_2-coated($Sr_4Al_{14}O_{25}$:Eu^{2+},Dy^{3+}) beads held in the dark state without light irradiation (marked as "Blank") varied little with time.

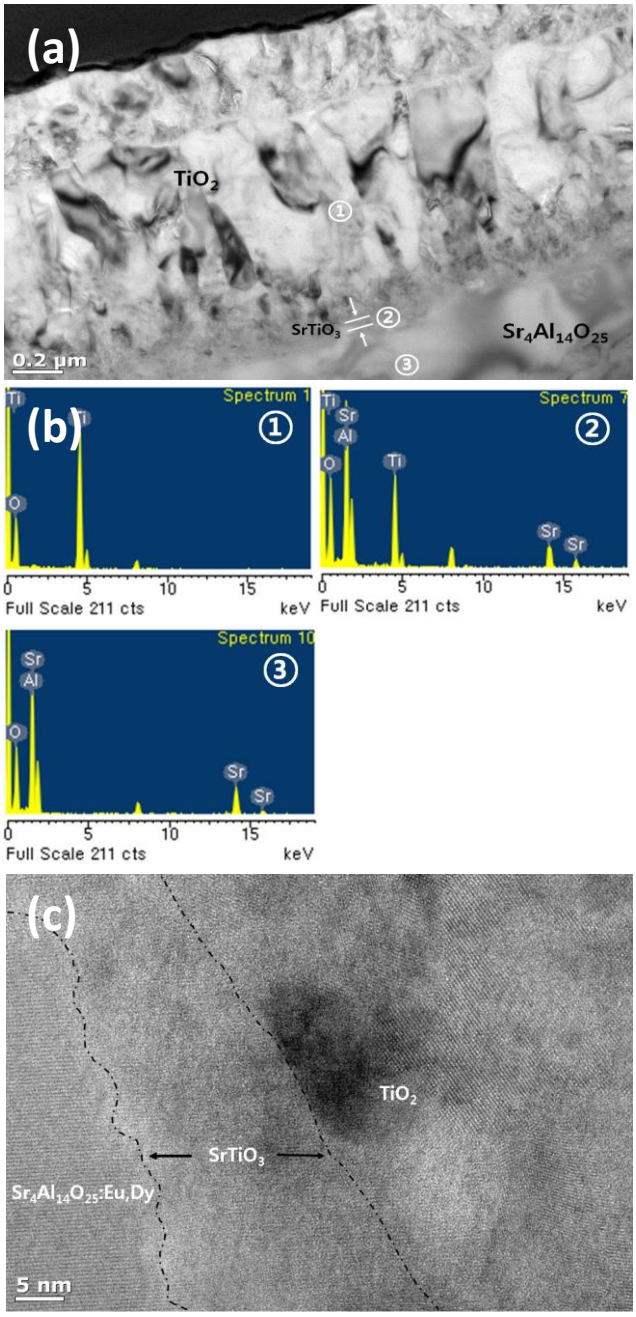

Fig. 3. (a) TEM cross-sectional image of the TiO_2-coated $Sr_4Al_{14}O_{25}$:Eu,Dy phosphor beads, (b) EDS spectra at three points marked in the TEM image in (a), and (c) magnified lattice image at the area of "②" marked in (a).

On the other hand, under both UV and visible light irradiation the benzene concentration decreased gradually with increasing irradiation time, indicating that the TiO_2-coated phosphor underwent a photocatalytic reaction. The benzene concentration under UV irradiation decreased slightly faster than that under visible light in the first half of the total irradiation time, but was similar to each other in the second half. **Fig. 4(b)** shows the change in toluene concentration with the irradiation time for the TiO_2 coated phosphor ($Sr_4Al_{14}O_{25}$:Eu^{2+},Dy^{3+}) beads under either UV or

visible light irradiation. Similar to benzene, the toluene concentration decreased gradually with increasing irradiation time.

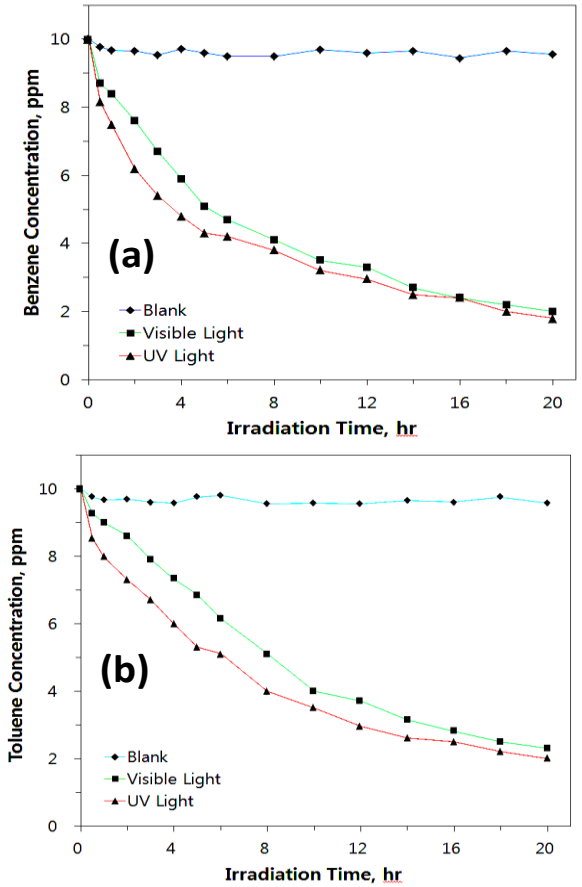

Fig. 4. Variations of (a) benzene and (b) toluene concentration with an irradiation time for the TiO_2 coated phosphor ($Sr_4Al_{14}O_{25}$:Eu^{2+},Dy^{3+}) beads under UV and visible light irradiations. The "Blank" symbol stands for the sample of TiO_2-($Sr_4Al_{14}O_{25}$:Eu^{2+},Dy^{3+}) beads held in the dark state without light irradiation.

Pure TiO_2 was photo-excited only under UV-light irradiation. Therefore, the light photons emitted from the ($Sr_4Al_{14}O_{25}$:Eu^{2+}, Dy^{3+}) phosphor might not have contributed to the photo-generation of electron-hole pairs because the wavelength was in the range of 410~600 nm. On the other hand, the intermetallic compound of $SrTiO_3$ might have formed through the intermixing of Ti and Sr atoms at the interface between TiO_2 and $Sr_4Al_{14}O_{25}$:Eu^{2+}, Dy^{3+} phosphor. $SrTiO_3$ has a perovskite-type structure with an energy band gap of approximately 3.2 eV [**28**], which is similar that of TiO_2 (3.03 eV for rutile and 3.18 eV for anatase). In the meantime, at the interface layer of $SrTiO_3$, the Sr ion occupies the Ti-site and creates an anion defect as shown in the following defect equation using the following Kröger–Vink notation:

$$Sr \xrightarrow{Ti} Sr''_{Ti} + V_O^{\cdot\cdot}$$
$$\text{or } O_O = V_O^{\cdot\cdot} + \frac{1}{2}O_2(g) + 2e'$$

where, Sr''_{Ti} and $V_O^{\cdot\cdot}$ are a divalent strontium on a titanium site and an oxygen vacancy, respectively. As Sr^{2+} is substituted for Ti^{4+}, an oxygen ion site is left vacant positively to maintain the electric neutrality. Also, one positive oxygen ion vacancy generates two negative electrons according to the above equation.

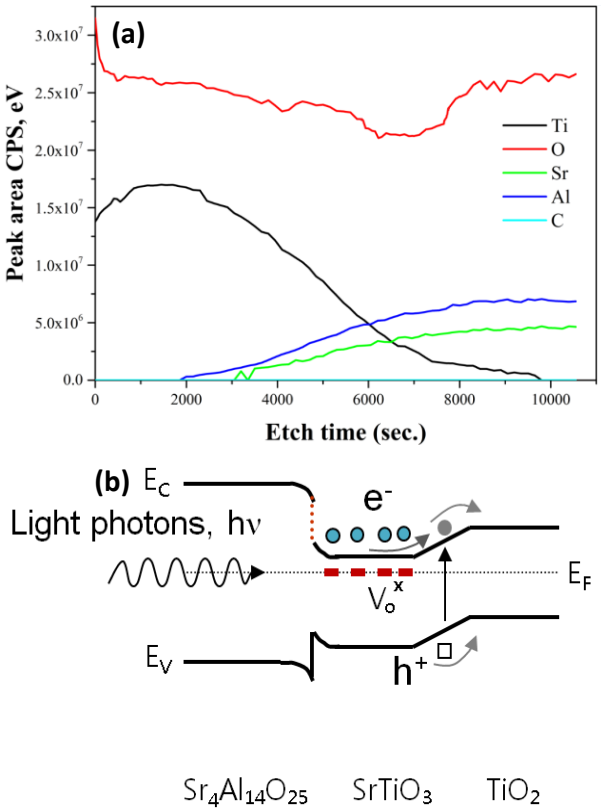

Fig. 5. (a) AES depth profile and (b) schematic energy band structure at the interface of the TiO_2-coated $Sr_4Al_{14}O_{25}$:Eu^{2+}, Dy^{3+}.

An AES depth profile was obtained in order to observe the compositional variations at the interface between TiO_2 and phosphor ($Sr_4Al_{14}O_{25}$:Eu^{2+}, Dy^{3+}) and shown in **Fig. 5(a)**. Referring to the oxygen element of the AES depth profile that decreased at the interface, the formation of oxygen vacancies was confirmed since oxygen decreased at the interface region between TiO_2 and phosphor ($Sr_4Al_{14}O_{25}$:Eu^{2+},Dy^{3+}). Thus, the defects in the oxygen vacancies occupy the localized levels below the conduction band in the band gap and give extra electrons that are subsequently excited to the conduction band by the photons emitted from the phosphor. The extra excited electrons in the conduction band can participate in a photocatalytic reaction, resulting in an enhancement of the photodecomposition of benzene (or toluene).

In addition, the junction of TiO_2 with $SrTiO_3$ with different Fermi levels (E_F) might induce energy band bending and shift the absorption band of titanium oxide toward the visible light region [**29, 30**]. The possible energy band structure at the interface between TiO_2 and phosphor is drawn schematically as shown in **Fig. 5(b)**. Therefore, the TiO_2-coated phosphor particles had a larger number of electron-hole pairs, which enhanced the photocatalytic reaction under visible irradiation. Once the energy bands at the junction area of the TiO_2-$Sr_4Al_{14}O_{25}$:Eu^{2+}, Dy^{3+} phosphor are activated by visible

light, the emitted light photons from the phosphors enable the photo-generation of electron-hole pairs, engaging the photocatalytic degradation of benzene (or toluene) gas.

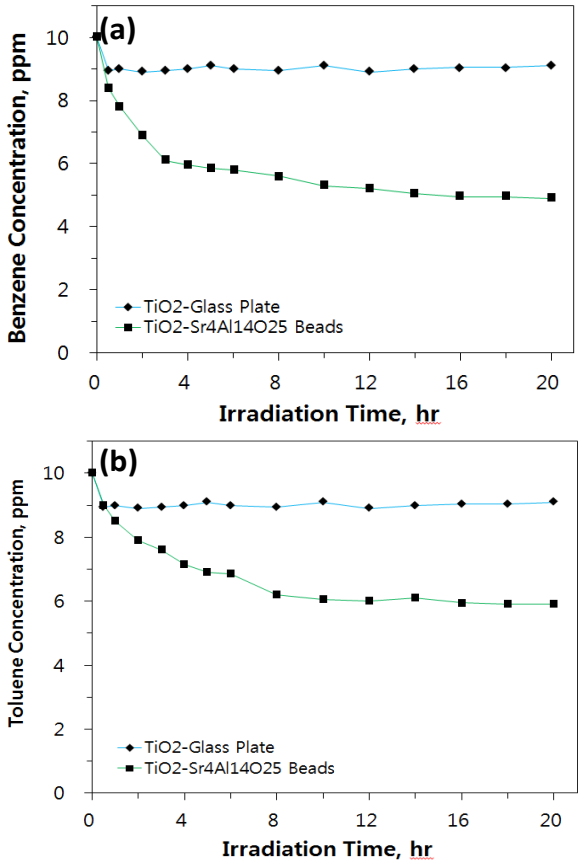

Fig. 6. Variations of (a) benzene and (b) toluene concentration with the irradiation time for the TiO_2 coated phosphor ($Sr_4Al_{14}O_{25}:Eu^{2+},Dy^{3+}$) beads and pure TiO_2(P-25) in the dark. The light was switched-off after 30 min irradiation. The thickness of the TiO_2-coated layer was approximately 150 nm.

Fig. 6 shows the changes in (a) benzene and (b) toluene concentration with time for the TiO_2 coated phosphor ($Sr_4Al_{14}O_{25}:Eu^{2+}$, Dy^{3+}) beads under darkness. For comparison, the concentration data obtained for pure TiO_2 (P-25, Degussa) were superimposed in the graphs. The samples were irradiated with UV light for 30 min, and then switched-off (dark state). The benzene concentration decreased slightly for pure TiO_2 after the light had been switched-off, indicating that pure TiO_2 was not photo-excited in the dark state. On the other hand, the benzene concentration continued to decrease moderately for the TiO_2-coated $Sr_4Al_{14}O_{25}:Eu^{2+},Dy^{3+}$ phosphor beads, even in the dark state. Similar to benzene, the toluene concentration for the TiO_2-coated $Sr_4Al_{14}O_{25}:Eu^{2+},Dy^{3+}$ phosphor beads decreased gradually with increasing holding time even after the light had been switched-off. This suggests that the TiO_2-coated $Sr_4Al_{14}O_{25}:Eu^{2+},Dy^{3+}$ phosphor beads is photo-reactive under the light photons emitted from the $Sr_4Al_{14}O_{25}:Eu^{2+},Dy^{3+}$ phosphor.

Conclusion

The TiO_2 thin film was deposited on phosphor beads of $Sr_4Al_{14}O_{25}:Eu^{2+}$, Dy^{3+} by LPCVD and its photocatalytic activity was investigated by measuring the degradation of benzene and toluene gases under either ultraviolet or visible light irradiation, as well as in the dark state. The LPCVD TiO_2-coated $Sr_4Al_{14}O_{25}:Eu^{2+}$, Dy^{3+} phosphor beads showed the photocatalytic degradation of benzene and toluene gases under visible light irradiation. The coupling of TiO_2 with $Sr_4Al_{14}O_{25}:Eu^{2+}$, Dy^{3+} phosphor might result in energy band bending in the junction region, which makes the TiO_2 crystal at the interface photo-reactive under visible light irradiation. The light photons emitted from the phosphors promoted the photo-generation of electron-hole pairs in the TiO_2-coated $Sr_4Al_{14}O_{25}:Eu^{2+}$, Dy^{3+} phosphors, and enhanced the photocatalytic activity of TiO_2. In addition, the intermetallic compounds of $SrTiO_3$ that are formed at the interface between TiO_2 and the $Sr_4Al_{14}O_{25}:Eu^{2+}$, Dy^{3+} phosphor may result in the formation of oxygen vacancies and additional electrons, subsequently promoting the photodecomposition of benzene (or toluene) gas. The LPCVD TiO_2-coated $Sr_4Al_{14}O_{25}:Eu^{2+}$, Dy^{3+} phosphor beads was photo-reactive in the dark through the light photons emitted from the $Sr_4Al_{14}O_{25}:Eu^{2+},Dy^{3+}$ phosphor. Benzene and toluene gases decomposed continuously on the TiO_2-coated $Sr_4Al_{14}O_{25}:Eu^{2+}$, Dy^{3+} phosphor beads for a considerable amount of time after the light had been switched-off (dark state).

Acknowledgements

This research was supported by Basic Science Research Program through the National Research Foundation of Korea (NRF) funded by the Ministry of Education (2010-0022715), and by a grant (14CTAP-C077607-01) from Infrastructure and transportation technology promotion research program funded by Ministry of Land, Infrastructure and Transport of Korean government.

Reference

1. Wang, J.; Sun, W.; Zhang, Z.; Jiang, Z.; Wang, X.; Xu, R.; Li, R.; Zhang, X.; *J. Colloid Interface Sci.*, **2008**, *320 (1)*, 202. **DOI**: 10.1016/j.jcis.2007.12.013
2. Liu, S. X.; Qu, Z. P.; Han, X. W.; Sun, C. L.; *Catal. Today*, **2004,** *93*, 877. **DOI**: 10.1016/j.cattod.2004.06.097
3. Lee, K.; Lee, N. H.; Shin, S. H.; Lee, H. G.; Kim, S. J.; *Mater. Sci. Eng. B*, **2006,** *129*, 109. **DOI**: 10.1016/j.mseb.2005.12.032
4. Yan, M. C.; Chen, F.; Zhang, J. L.; Anpo, M.; *J. Phys. Chem. B*, **2005,** *109*, 8673. **DOI**: 10.1021/jp046087i
5. Bessekhouad, Y.; Robert, D.; Weber, J.-W.; *Catal. Today*, **2005,** *101(3-4)*, 315. **DOI**: 10.1016/j.cattod.2005.03.038
6. Sano, T.; Mera, N.; Kanai, Y.; Nishimoto, C.; Tsutsui, S.; Hirakawa, T.; Negishi, N.; *Appl. Catal. B: Environ.*, **2012**, *128*, 77. **DOI**: 10.1016/j.apcatb.2012.06.034
7. Asahi, R.; Morikawa, T.; Ohwaki, T.; Aoki, K.; Taga, Y.; *Science*, **2001**, *293*, 269. **DOI**: 10.1126/science.1061051
8. Anderson, C.; Bard, A. J.; *J. Phys. Chem. B*, **1997**, *101(14)*, 2611. **DOI:** 10.1021/jp9626982
9. Shchukin, D.; Poznyak, S.; Kulak, A.; Pichat, P.; *J. Photochem. Photobiol. A:Chem.* **2004**, *162(1-2)*, 423. **DOI**: 10.1016/S1010-6030(03)00386-1
10. Zhu, L.; Meng, Z.-D.; Cho, K.-Y.; Oh, W.-C.; *New Carbon Materials*, **2012**, *27(3)*, 166. **DOI**: 10.1016/S1872-5805(12)60011-0
11. Bessekhouad, Y.; Brahimi, R.; Hamdini, F.; Trari, M.; *J. Photochem. Photobiol. A: Chem.*, **2012**, *248*, 15. **DOI**: 10.1016/j.jphotochem.2012.08.013
12. Li, H. H.; Yin, S.; Wang, Y.; Sato, T.; *J. Catal*, **2012**,. *286*, 273. **DOI**: 10.1016/j.jcat.2011.11.013

13. Sannino, D.; Vaiano, V.; Ciambelli, P.; *Catal. Today*, **2013**, *205*, 159.
DOI: 10.1016/j.cattod.2012.07.038
14. Kim, J.-S.; Kim, S.-W.; Jung, S.-C.; *J. Nanosci. Nanotech.*, **2014**, *14(10)*, 7751.
DOI: 10.1166/jnn.2014.9426
15. Blasse, G.; Grabmaier, B. C.; Luminescent Materials, Springer, Berlin,**1994**.
16. Kumar Vinay; Bedyal A. K.; Sharma J.; Kumar V.; Ntwaeaborwa O. M.; Swart H. C.; *Appl. Phys. A*, **2014**, *116*, 1785.
DOI: 10.1007/s00339-014-8331-5
17. Kumar N.; Kumar V.; Swart H.C.; Mishra A. K.; Ngila J. C.; Parashar V.; *Mater. Lett.*, **2015**, *146*, 51.
DOI: 10.1016/j.matlet.2015.01.150
18. Nakazawa, E.; Mochida, T.; *J. Luminescence*, **1997**, *72–74*, 236.
DOI: 10.1016/S0022-2313(97)00043-4
19. Sakai, R.; Katsumata, T.; Komuro, S.; Morikawa, T.; *J. Luminescence*, **1999**, *85*, 149.
DOI: 10.1016/S0022-2313(99)00061-7
20. Shen, C.; Wang, Y.J.; Xu, J.H.; Luo, G.S.; *Chem. Eng. J.*, **2012**, *209*, 478.
DOI: 10.1016/j.cej.2012.08.044
21. Keller, N.; Rebmann, G.; Barraud, E.; Zahraa, O.; Keller, V.; *Catal. Today*, **2005**, *101(3)*, 323.
DOI: 10.1016/j.cattod.2005.03.021
22. Xu, Y.; Langford, H.; *J. Phys. Chem.*, **1995**, *99 (29)*, 11501.
DOI: 10.1021/j100029a031
23. Kim, S.-W.; Kim, J.-S.; *Kor. J. Met. Mater.*, **2011**, *49(4)*, 348.
DOI: 10.3365/KJMM.2011.49.4.348
24. Kim, B.-J.; Hasan, Z.; Kim, J.-S.; *J. Ceram. Proc. Res.*, **2013**, *14(5)*, 601.
25. Kim, B.; Byun, D.; Lee, J.-K.; Park, D.; *Jpn. J. Appl. Phys.*, **2002**, *41*, 222.
DOI: 10.1143/JJAP.41.222
26. Byun, D.; Jin, Y.; Kim, B.; Lee, J.K.; Park, D.; J. *Hazard. Mater.* B, **2000** ,*73*, 199.
DOI: 10.1016/S0304-3894(99)00179-X
27. Sibai, A.; Lhostis, S.; Rozier, Y.; Salicio, O.; Amtablian, S.; Dubois, C.; Legrand, J.; Sénateur, J.P.; Audier, M.; Hubert-Pfalzgraff, L.; Dubourdieu, C.; Ducroquet, F.; *Microelec. Reliability*, **2005**, *45(5)*, 941.
DOI: 10.1016/j.microrel.2004.11.020
28. Miyauchi, M.; Takashio, M.; Tobimatsu, H.; Langmuir, **2004**, *20*, 232.
DOI: 10.1021/la0353125
29. Otsuka-Yao-Matsuo, S.; Ueda, M.; *J. Photochem. Photobiol. A:Chem.*, **2004**, *1*,168,.
DOI: 10.1016/j.jphotochem.2004.04.022
30. Yoon, J.-H.; Jung, S.-C.; Kim, J. S.; *Mater. Chem. Phys.*, **2011**, *125*, 342.
DOI: 10.1016/j.matchemphys.2010.11.004

